Journal of Pharmaceutical and Applied Chemistry

ISSN: 2357-0210 VOLUME 3, ISSUES 2, 2017 www.egyptfuture.org/ojs/

Electrochemical Concern for Biological Activity Displayed by Core–Shell Type Nanocomposites of $FeFe_2O_4$ & Ag^0 Family

Gennadii A. Dolynskyi [1,*], *Olena M. Lavrynenko* [1], *Oksana S. Krupennikova* [2] and *Yuriy K. Pirskyy* [2].

[1]Nanocomposites for Biomedicine Research Group, I. M. Frantsevich Institute for Problems of Material Science, National Academy of Sciences of Ukraine, 3 Krzhizhanovsky Street, 03680, Kyiv, Ukraine.

[2]Materials for Electrochemical Energetics Laboratory, V.I. Vernadskii Institute of General and Inorganic Chemistry, National Academy of Sciences of Ukraine, 32 – 34 Palladina Avenue, 03680, Kyiv, Ukraine.

Received: 17 May 2017, Revised: 1 Aug. 2017, Accepted: 4 Aug. 2017.
Published online: 1 Sep. 2017.

Abstract: The kinetic characteristics of oxygen reduction on the surface of core–shell type nanocomposites $FeFe_2O_4$ & Ag^0 are considered in the context of the certain catalytic cycle, which may occur due to electrochemical interaction between core and shell moiety. Being synthesized under different initial concentrations of Ag^+ in the incubation medium, metal silver nanoclusters on the surface of magnetite core can form a layer varying from islet-like structures to aggregated spherical porous shell, thereby altering the electrocatalytic activity of the nanocomposite. Consequently, the ability for reactive oxygen species generation can be predetermined to specify potential biological activity of the nanocomposite through its interference with free radical metabolism.
Keywords: Core–shell type nanocomposites, Argentum ions, Ferrous ferric oxide, Oxygen electroreduction.

.

1 Introduction

Various nanosized structures comprising metallic or ion silver became widespread during last decade [1]. Mostly, these compounds are exploiting as antimicrobials, which are efficient against different kinds of pathogens (bacteria, fungi, protozoa, etc.) including those with high resistance to antibiotics [2, 3]. Despite constantly increasing evidence of the silver nanoparticles cellular effects, both in pro- and eukaryotes the mechanisms of their biological activity remain not fully understood [4]. Commonly, it is believed to be related to argentum ions formation at the nanoparticles surface in biological media [5]. To confirm this viewpoint the supporters emphasize a possibility of Ag^+ release from nanoparticulate silver under the aerobic conditions due to Ag^0 oxidation on the nanoparticle surface (Eqs. 1, 2):

$$4\,Ag^0 + O_2 \rightarrow 2Ag_2O \quad (1)$$

$$2Ag_2O + 4H^+ \rightarrow 4Ag^+ + 2H_2O \quad (2)$$

thereby concluding that toxicity of silver nanoparticles can be explained only by the dose-response of the released Ag^+ [6, 7].

Meanwhile, recent findings related to oxygen reduction on silver nanoparticles demonstrated the formation of significant amounts of hydrogen peroxide [8]. Electrocatalytic reduction of molecular oxygen can be conducted either by a direct path to water (Eq. 3) [9]:

$$O_2 + 4H_2O + 4e^- \rightarrow 2H_2O + 4OH^- \quad (3)$$

or by a series of two electrons transferred at a time with hydrogen peroxide as an intermediate (Eqs. 4-5) [10]:

$$O_2 + 2H_2O + 2e^- \rightarrow H_2O_2 + 2OH^- \quad (4)$$

$$H_2O_2 + 2H_2O + 2e^- \rightarrow 2H_2O + 2OH^- \quad (5)$$

It was demonstrated that at silver cathodes the oxygen reduction follows 2+2 pathway, where the H_2O_2 electrogenerated can either diffuse away from the electrode surface or be reduced to water [11].

As the reduction of O_2 is limited by diffusion rate of H_2O_2, which becomes considerably increased at nanoscale [12], then the dissolution of Ag^0 (Eq. 6) is driven here by the reaction in Eq. (7):

$$Ag^0 \rightleftarrows Ag^+ + e^- \quad (6)$$

$$O_2 + 2H^+ + 2e^- \rightleftarrows H_2O_2 \quad (7)$$

As the matter of fact, this insight provides electrochemical processes where the reactive oxygen species occur and play significant role contributing to bactericidal activity of nanoparticulate silver concurrently with Ag^+. Therefore, we can also explain versatile activity of $FeFe_2O_4$ & Ag^0 nanocomposites formed under various argentum content that have showed both prooxidant or radical scavenging and immunomodulating properties [13, 14].

The objective of the present study was to assess putative electrochemical interaction between core and shell moiety of the nanocomposites $FeFe_2O_4$ & Ag^0, which can specify their behavior in biological environment.

2 Materials and methods

2.1 Rotation-corrosion dispergation procedure

We used nanostructures with magnetite core and metal silver shell that produced by means of the rotation-corrosion dispergation procedure, which had described in details previously [15].

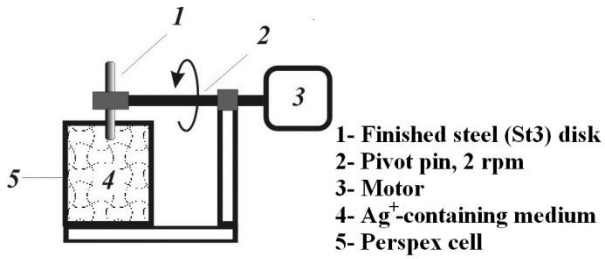

Figure 1. Schematics of the rotation-corrosion dispergation procedure.

In brief, slowly rotating disk made of finished steel (St3) was immersed into dispersion medium up to one-third of its diameter, with other two-thirds exposed to ambient atmosphere (**Figure 1**). As the dispersion medium, aqueous solution of $AgNO_3$ was used, varying Ag^+ concentration from 0.5 mg to 20.0 mg per liter and pH value at the range of 2.5 to 12.0.

2.2 Structural analysis of obtained nanocomposites

2.2.1 X-ray diffraction analysis (XRDA)

To perform XRDA we used the instrumentality of DRON 3 computerized equipment with filtered emission of cobalt anode. The velocity of plotting was $1° \cdot min^{-1}$; the critical Wolf–Bragg's angle was 80 °.

2.2.2 X-ray fluorescence spectroscopy (XRFS)

The instrumentality was ELVAX spectrometer with the titanium anode.

2.3 Electrochemical analyses

2.3.1 Measuring equipment

In electrochemical experiments we exploited three-electrode setup with separated cathode and anode spaces, main gas-diffusion 'floating' electrode and silver chloride electrode as a reference. The device was connected to potentiostat PI–50–1.1 (Gomel Plant of Measuring Devices, Gomel, Republic of Belarus) and digital multimeter with USB-interface AXIOMET AX–18B.

The gas-diffusion 'floating' electrode was designed as 10 mm diameter cylindrical flat tablet, 2 mm thick, 0.95 g / cm^3 density, with nickel wire attached as a current collector. The tablet was made by pressing at 5 – 7 MPa of carbon black P–803 (Russian standard GOST 7885–86) mixture with water emulsion of polytetrafluorethylene FP–4D (Russian standard TU 6–05–12–46–76) added up to 30 wt. % for hydrophobization. This main electrode was modified before each testing procedure by application of a sample nanocomposite up to 1 mg per cm^2, then pressing at 5 – 6 MPa to form monolayer coating. This arrangement ensured equal supply of oxygen to the outer surface of grains of the catalyst providing fairness of oxygen consumption and kinetic mode for reaction [16, 17].

2.3.2 Electrochemical measurements

As a stock electrolyte we used 1 M KOH solution thermostatted at 20 °C under ambient air. Such conditions enable complete four-electron transfer due to enhanced decomposition of peroxide intermediate on the active catalytic sites [18]. Polarization curves for oxygen electroreduction reaction on the nanocomposites-modified electrode were recorded at controlled potential mode with 10 mV steps. The catalytic activity of $FeFe_2O_4$ & Ag^0 nanocomposites was quantified analyzing consequent current-potential patterns by following criteria: stationary potential, E_{st} (V); slopes of polarization curves, b_1 and b_2 (V); exchange current j_0 (A / g); electrocatalytic activity of $FeFe_2O_4$ & Ag^0 nanocomposites, j (A / g) under the constant potential E (V).

3 Results

3.1 Structural features of obtained nanocomposites

The production procedure resulted in obtaining of various nanostructures that differed in size and shape depending on pH and initial argentum ions concentration in the system.

3.1.1 XRD characteristics of the nanostructures

Among reflexes on XRD-patterns we identified those corresponding to magnetite, lepidocrocite, and silver within all the range of argentum ions concentrations (**Figure 2**).

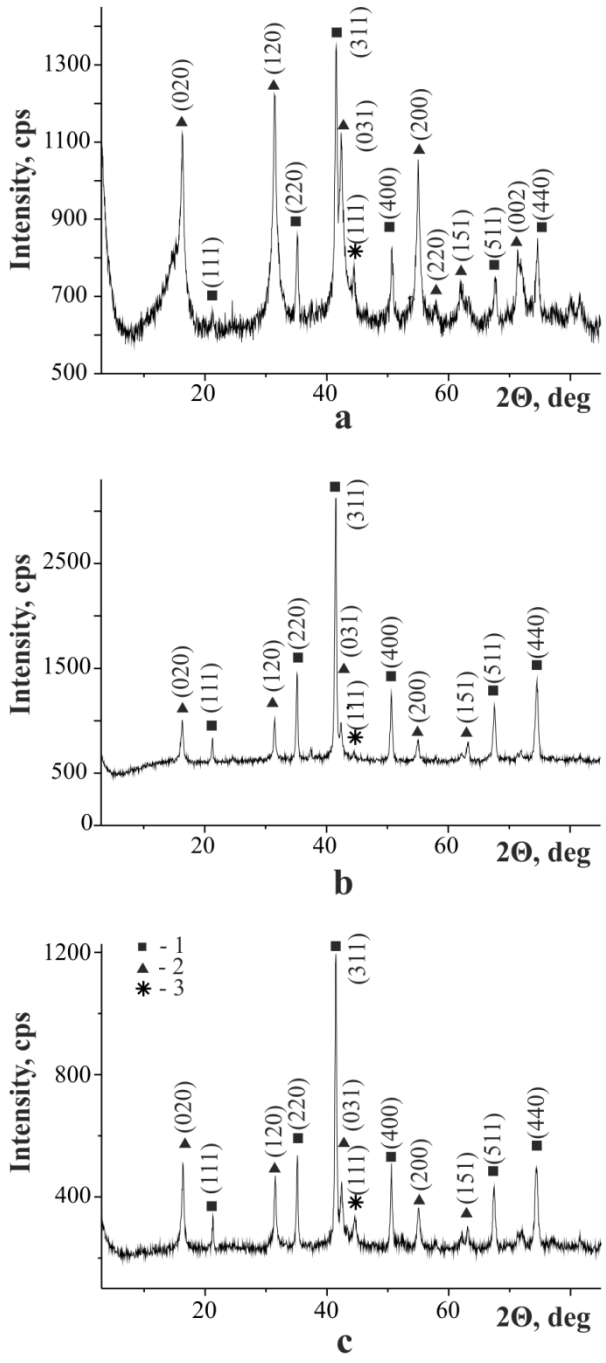

Figure 2. XRD patterns of $FeFe_2O_4$ & Ag^0 nanocomposites formed under different Ag^+ concentration: 0.5 (a), 5.0 (b) and 20 (c) mg / l; ■ – magnetite, ▲ – lepidocrocite and * – silver.

Based on the maximal amplitudes of the reflexes, relative magnetite and lepidocrocite content was calculated and plotted for each of Ag^+ concentrations (**Figure 3**).

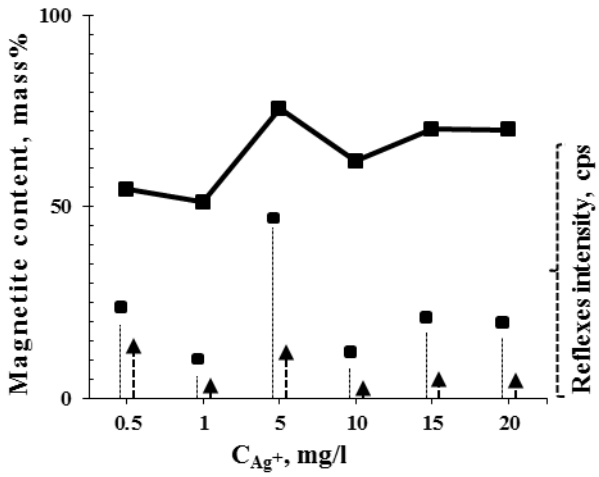

Figure3. Magnetite content by XRDA among two iron-bearing phases: ■ – magnetite (311) and ▲ – lepidocrocite (020) after the nanocomposites formation under different argentum concentrations (C_{Ag^+}) in dispersion medium.

The diagram demonstrates evident singularity at Ag^+ concentration of 5.0 mg per liter, probably related to the process of shell forming. Mean crystalline size calculated by Scherer's formula ranged from 19.5 nm to 27.0 nm, showing tendency to growth with increase in the initial argentum ions concentration.

3.1.2 XRFS characteristics of the nanostructures

XRFS data showed both argentum and iron atoms exposed on the surface of nanoparticles, that partition changed depending on the source argentum ions concentration, too (**Figure 4**).

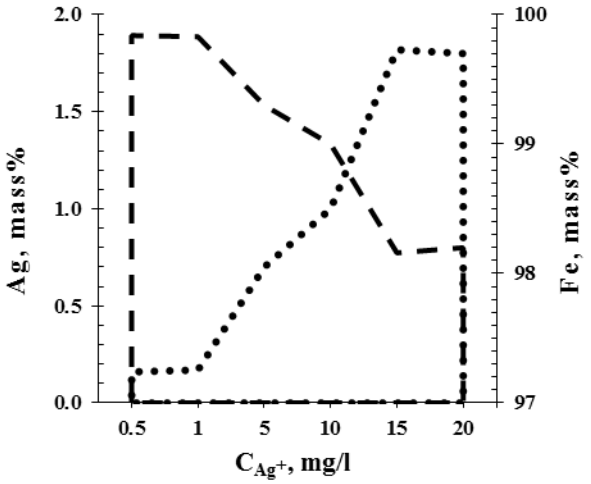

Figure 4. Mass fractions of argentum (•) and iron (—) in $FeFe_2O_4$ & Ag^0 nanocomposites formed under different Ag^+ concentration (C_{Ag^+}) in the dispersion medium.

3.2 Electrochemical behavior of the nanocomposites

3.2.1 Polarization patterns

Polarization curves under the main electrode modifications by the $FeFe_2O_4$ & Ag^0 nanocomposites varied along with initial argentum ions concentration in dispersion medium for the nanocomposites formation (**Figure 5).**

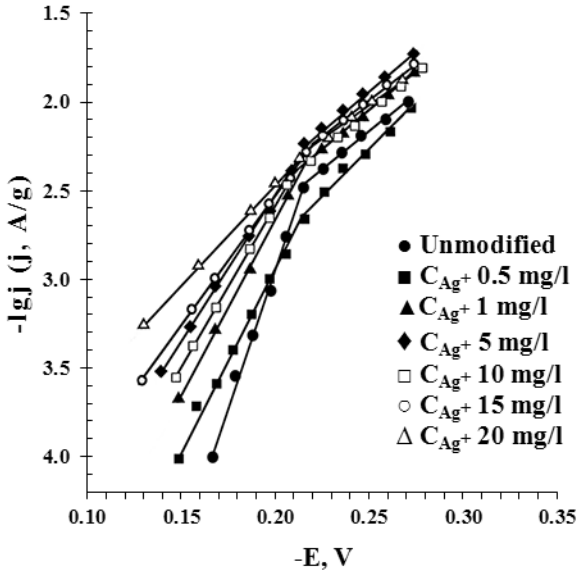

Figure 5. Series of polarization curves for main electrode modifications by $FeFe_2O_4$ & Ag^0 nanocomposites, which were formed under different Ag^+ concentration (C_{Ag^+}) in the dispersion medium.

Generally, the slopes of obtained polarisation curves were similar to those demonstrated for electrocatalysis on the carbon-based materials [19]. Notably, the modification of main electrode by the nanocomposite formed under the highest Ag^+ concentration of 20 mg per liter was followed by the largest positive potential shift of the polarization curve, as well as the highest exchange current density.

Plotting exchange current values vs. series of increasing Ag^+ concentrations that were used to form consequent nanocomposites, demonstrated apparent relation between electrochemical activity and specialty of the nanostructure (**Figure 6**).

3.2.2 Electrokinetic parameters

Calculation data derived from the polarization curves analysis, made it possible to obtain kinetic parameters of oxygen electroreduction on different $FeFe_2O_4$ & Ag^0 nanocomposites that are summarized in **Table 1**.

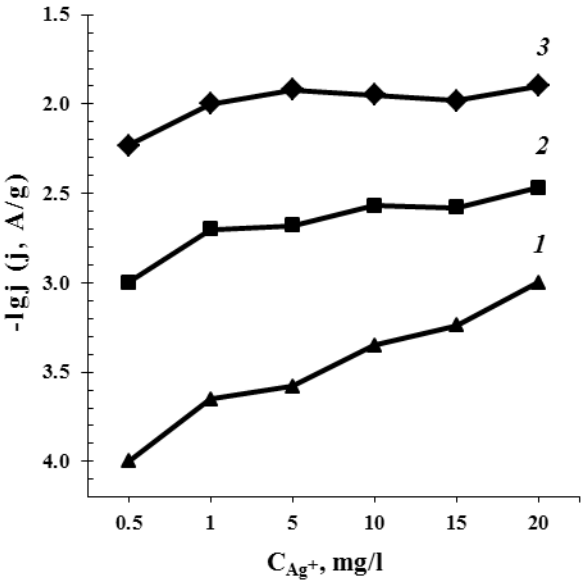

Figure 6. Increase in exchange current due to enhanced activity for oxygen electroreduction over the catalysis on $FeFe_2O_4$ & Ag^0 depending on argentum ions concentration (C_{Ag^+}) used to form the nanocomposites; records upon different E = - 0.15 (*1*), - 0.20 (*2*) and - 0.25 (*3*) V.

Table 1. Kinetic parameters for oxygen reduction reaction on $FeFe_2O_4$ & Ag^0-modified electrodes.

C_{Ag^+}, mg / l	E_{st}, V	$\partial E/\partial lgj$, V		Exchange current j_0, A / g
		b_1	b_2	
Unmodified	-0.121	0.065	0.126	$1.0 \cdot 10^{-4}$
0.5	-0.142	0.058	0.101	$1.1 \cdot 10^{-3}$
1	-0.137	0.057	0.128	$1.4 \cdot 10^{-3}$
5	-0.130	0.057	0.110	$1.2 \cdot 10^{-3}$
10	-0.110	0.067	0.122	$1.1 \cdot 10^{-3}$
15	-0.101	0.074	0.132	$1.5 \cdot 10^{-3}$
20	-0.094	0.090	0.134	$1.7 \cdot 10^{-2}$

C_{Ag^+} – initial concentration of Ag^+ ions in the dispersion medium for the specific nanocomposite formation.

4 Discussion

Distribution of argentum and iron phases during the nanocomposites formation shows alteration of the process when initial Ag^+ concentration in the dispersion medium becomes 5.0 mg per liter (**Figure 4** and **Figure 5**). Applying the data of the nanocomposites' structural analysis to explanation of the electrochemical phenomena,

two subgroups can be distinguished among the $FeFe_2O_4$ & Ag^0 nanocomposites family. The first one, specific to nanocomposites with Ag^+ content up to 5.0 mg per liter and the second one, which is specific to nanocomposites formed under the Ag^+ concentration of 10 to 20 mg per liter. These may suggest evolution from islet-like structures all over the core to aggregated spherical porous shell, which occur following the increase in Ag^+ concentration.

The rate of exchange current, as well as Tafel slopes indicate the prevalence of oxygen reduction through a two-electron pathway with hydrogen peroxide formation. Nevertheless, combined mechanism of oxygen reduction may take place, too, which run both through hydrogen peroxide generation (Eqs. 8 – 10) and partly through a four-electron pathway (Eq. 11):

$$O_2 + H_2O + 2\,e^- = HO_2^- + OH^- \quad (8)$$

with subsequent stage either of hydroperoxyl electroreduction:

$$HO_2^- + H_2O + 2\,e^- = 3\,OH^- \quad (9)$$

or chemical reaction of disproportionation:

$$HO_2^- = OH^- + \tfrac{1}{2}\,O_2, \quad (10)$$

concurrently, four electrons can be transferred to an oxygen at once:

$$O_2 + 2\,H_2O + 4\,e^- = 4\,OH^-. \quad (11)$$

Though iron can catalyze oxygen reduction through hydrogen peroxide generation, the catalytic activity will be significantly enhanced by argentum. Thereafter minimal and maximal values of exchange current fit with the lowest (0.5 mg per liter) and the highest (20 mg per liter) Ag^+ concentrations, respectively, but the relation is non-linear at the intermediate range. Apparently, the initial increase in exchange current occurs due to Ag^+ incorporation into $FeFe_2O_4$ crystallites, while further formation of silver metal nanoclusters on the surface of magnetite until accomplished core & shell nanostructure is followed by the exchange current plateau (Curve 2 and Curve 3 in **Figure 6**). Probably, under low argentum concentrations the reduction of oxygen on $FeFe_2O_4$ takes place directly at structure imperfections comprising active sites. In this case assumed oxygen reduction cycle occurs on the $FeFe_2O_4$ surface due to cation vacancies. After oxygen adsorption onto these sites a cation vacancy draws electron off the metal salt in oxide structure and changes its oxidation level. Joining the electrochemical system, the electron readily recovers valence of metal in oxide thereby forcing an electron transfer onto oxygen and thus formation of peroxide species $^-O–O^-$. Consequently, cation vacancies at iron oxide core of the composite maintain oxygen electroreduction, which courses to aqua via intermediate hydrogen peroxide formation. The cycle of oxygen reduction can be either pure electrochemical (I) or mixed (II), with chemical reaction of H_2O_2 disproportionation (**Figure 7**).

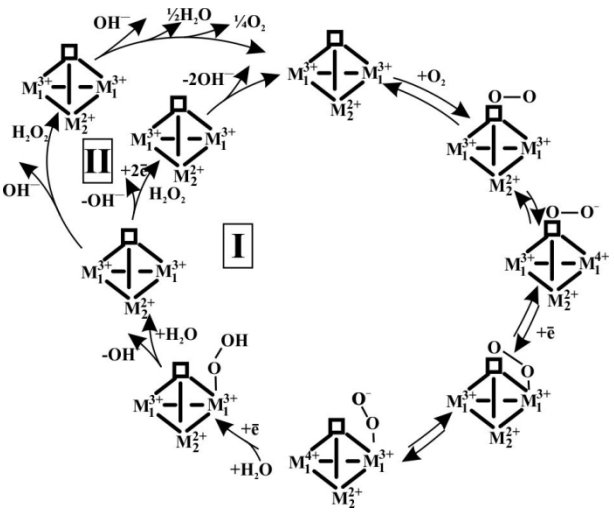

Figure 7. Assumed oxygen reduction cycles, which occur on the nanocomposite due to surface cation vacancies at $FeFe_2O_4$ core: I – O_2 electroreduction via H_2O_2 formation, II – O_2 electroreduction with chemical reaction of H_2O_2 disproportionation.

Under the higher argentum concentrations multiple silver nanoclusters on the iron oxide surface begin acting as centers for oxygen reduction providing more intricate catalytic cycle (**Figure 8**).

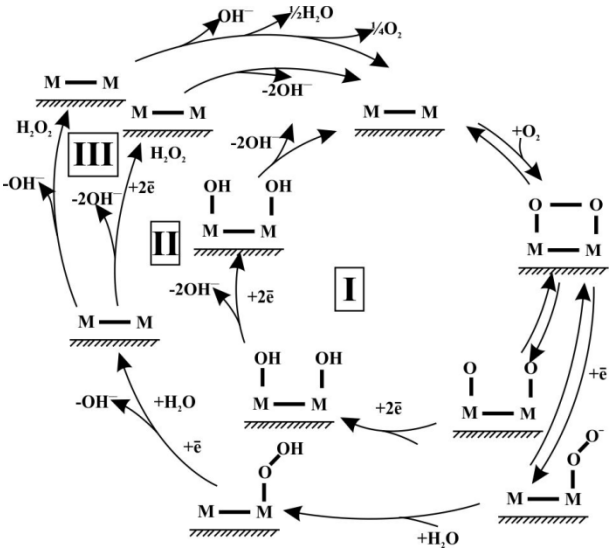

Figure 8. Assumed oxygen reduction cycles, which occur on argentum clusters comprising the shell on $FeFe_2O_4$ core of the nanocomposite: I – direct electroreduction of O_2 to H_2O, II – electroreduction of O_2 via H_2O_2 formation that may be completed with chemical H_2O_2 disproportionation – III.

At the beginning of the reduction on silver nanoclusters a chemosorption of oxygen onto argentum takes place. Then, two pathways could occur: the first-one, through a rupture of –O–O– bond and formation of oxide structures on the surface (I), and the second, electrochemical-one through electron bonding and formation of peroxide species $^{-}O–O^{-}$ (II). Pathway (I) results in direct electroreduction of O_2 to H_2O and pathway (II) yields electrochemical reduction of O_2 via H_2O_2. Afterwards, a reaction of hydrogen peroxide disproportionation onto H_2O and O_2 is possible (III).

The cycle of oxygen reduction terminates with water synthesis and complete regeneration of the surface that is ready for next cycle.

The existence of various concurrent cycles could explain the slopes of polarization curves observed under oxygen electroreduction. Consequently, a contribution of certain catalytic cycle is specified by electrochemical interaction between core and shell moiety that may differ depending on the nanocomposite formation conditions.

Extrapolation of these processes to near-neutral pH range supposes the two-electron reduction to be the only reaction pathway. After anion desorption both pathways ($2\,e^{-}$ and $4\,e^{-}$) are feasible and relative contribution of each is determined by the surface concentration of active argentum sites required for the catalytic four-electron reduction pathway [20].

The reasoning presented above asserts the crucial role of argentum nanoclusters' density on ferrous/ferric oxide core for the oxygen reduction reactions that is similar to mechanism providing generation of reactive oxygen species on the silver nanoparticle interface [21].

4 Conclusion

The interaction between core and shell moiety of the $FeFe_2O_4$ & Ag^0 nanocomposites is a valuable clue for interpreting their behavior in aqueous oxygenated medium. Being synthesized under different initial concentrations of Ag^+ in the incubation medium, metal silver nanoclusters on the surface of magnetite core can form a layer varying from islet-like structures to aggregated spherical porous shell. Consequently, their electrocatalytic activity for oxygen reduction reactions modifies and enables pathways leading to generation of reactive oxygen species. Ultimately, the streamlined catalytic pathways, which are specific for certain nanocomposite of the $FeFe_2O_4$ & Ag^0 family, arise from Ag^+ interaction with iron oxide phases. The latter occurs firstly during the synthesis procedure, thus 'programming' the nanocomposite's potential biological activity due to their ability for the reactive oxygen species release, which may interfere with free radicals metabolism. While in biological environment, this activity will be kept as long as the catalytic capacity of the nanocomposite provides it. Then, it could be exhausted or even reversed because of alteration in the balance of innate redox systems comprising ferric/ferrous oxide core and metal silver shell of the nanocomposite.

Acknowledgement

This paper has been presented at the 4th International Conference "Nanotechnologies", October 24 – 27, 2016, Tbilisi, Georgia (Nano – 2016).

References

[1] R. Behra, L. Sigg, M.J.D. Clift, F. Herzog, M. Minghetti, B. Johnston, A. Petri–Fink, B. Rothen–Rutishauser. Bioavailability of silver nanoparticles and ions: From a chemical and biochemical perspective. *J. R. Soc. Interface* **10**, 0396 (2013).

[2] D.G. Romero–Urbina, H.H. Lara, J.J. Velázquez–Salazar, M.J. Arellano–Jiménez, E. Larios, A. Srinivasan, J.L. Lopez–Ribot, M.J. Yacamán. Ultrastructural changes in methicillin-resistant Staphylococcus aureus induced by positively charged silver nanoparticles. *Beilstein J. Nanotechnol*. **6**, 2396-2405 (2015).

[3] X. Dai, Q. Guo, Y. Zhao, P. Zhang, T. Zhang, X. Zhang, C. Li. Functional silver nanoparticle as a benign antimicrobial agent that eradicates antibiotic-resistant bacteria and promotes wound healing. *ACS Appl. Mater. Interfaces* **8** (39), 25798-25807 (2016).

[4] J. Wang, J. Li, G. Guo, Q. Wang, J. Tang, Y. Zhao, H. Qin, T. Wahafu, H. Shen, X. Liu, X. Zhang. Silver-nanoparticles-modified biomaterial surface resistant to staphylococcus: new insight into the antimicrobial action of silver. *Sci. Rep.* **6**, 32699 (2016).

[5] C. Volker, M. Oetken, J. Oehlmann. The biological effects and possible modes of action of nanosilver. *Rev. Environ. Contam. Toxicol.* **223**, 81-106 (2013).

[6] Z.-M. Xiu, J. Ma, P.J.J. Alvarez. Differential effect of common ligands and molecular oxygen on antimicrobial activity of silver nanoparticles versus silver ions. *Environ. Sci. Technol.* **45**, 9003-9008 (2011).

[7] Z.-M. Xiu, Q.-B. Zhang, H.L. Puppala, V.L. Colvin, P.J.J. Alvarez. Negligible particle-specific antibacterial activity of silver nanoparticles. *Nano Lett.*, **12** (8), 4271-4275 (2012).

[8] B.J. Plowman, K. Tschulik, E. Walport, N.P. Young, R.G. Compton. The fate of nano-silver in aqueous media. *Nanoscale* **7**, 12361-12364 (2015).

[9] L. Tammeveski, H. Erikson, A. Sarapuu, J. Kozlova, P. Ritslaid, V. Sammelselg, K. Tammeveski. Electrocatalytic oxygen reduction on silver nanoparticle/multi-walled carbon nanotube modified glassy carbon electrodes in alkaline solution. *Electrochem. Commun*. **20**, 15-18 (2012).

[10] N.A. Yashtulov, A.A. Revina, V.R. Flid. The mechanism of oxygen catalytic reduction in the presence of platinum and silver nanoparticles. *Russ. Chem. Bull*. **59**, 1488-1494 (2010).

[11] C.M. Sánchez-Sánchez, A.J. Bard. Hydrogen peroxide production in the oxygen reduction reaction at different electrocatalysts as quantified by scanning electrochemical microscopy. *Anal. Chem.* **81**, 8094-8100 (2009).

[12] C.C.M. Neumann, E. Laborda, K. Tschulik, K.R. Ward, R.G. Compton. Performance of silver nanoparticles in the catalysis of the oxygen reduction reaction in neutral media: Efficiency limitation due to hydrogen peroxide escape. *Nano Res*. **6**, 511-524 (2013).

[13] G.A. Dolynskyi, O.M. Lavrynenko. The ability of silver-based magnetite nanoparticles to attenuate lipid peroxidation in lecithin-containing model system. In: Interactions of Biogenic and Abiogenic Components in Natural and Anthropogenic Systems. Saint Petersburg, VVM Publ., 231-235 (2011).

[14] G.A. Dolynskyi, O.M. Lavrynenko, V.V. Nosov. Anti-inflammatory properties of nanocomposite $FeFe_2O_4$ & Ag^0 in experimental peritonitis. *Odessa Med. J.* **142** (2**)**, 10-14 (2014).

[15] O.M. Lavrynenko. Physicochemical properties of the $FeFe_2O_4$ & Ag^0 nanocomposites formed on the steel surface contacting with $AgNO_3$ water solutions in open-air system. *Nano Studies* **5**, 27-40 (2012).

[16] G.V. Shteinberg, I.A. Kukushkina, V.S. Bagotskii, M.R. Tarasevich. Kinetics of oxygen reduction at disperse carbon materials. *Soviet Electrochem*. **15 (4)**, 443-448 (1979).

[17] A.L. Wijnoltz. Floating electrode technique. In: Oxygen Reduction Catalysed by Carbon Supported Metal Chelates. Eindhoven, Tech. Univ. Eindhoven, 63-75 (1995).

[18] N. Ramaswamy, S. Mukerjee. Fundamental mechanistic understanding of electrocatalysis of oxygen reduction on Pt and non-Pt surfaces: Acid versus alkaline media. *Adv. Phys. Chem.* **2012**, 491604, 1-17 (2012).

[19] M.R. Tarasevich, V.A. Bogdanovskaya. The surface-modified carbon materials for electrocatalysis. *Usp. Khim*. **56** (7), 1139-1166 (1987).

[20] B.B. Blizanac, P.N. Ross, N.M. Markovic. Oxygen electroreduction on Ag(111): The pH effect. *Electrochim. Acta* **52**, 2264-2271 (2007).

[21] C. Batchelor-McAuley, K. Tschulik, C.C.M. Neumann, E. Laborda, R.G. Compton. Why are silver nanoparticles more toxic than bulk silver? Towards understanding the dissolution and toxicity of silver nanoparticles. *Int. J. Electrochem. Sci*. **9**, 1132-1138 (2014).